applied sciences

MDPI

Article

Study on the Performance of K-Type Pre-Embedded Iron Seat for Double-Slip Turnouts

Zeyu Wu [1], Dongsheng Yang [2,3], Zhongyuan Wang [2,3], Meng Wang [2,3], Zelin Chen [2,3], Zhenhua Zhao [2,3,*] and Pu Wang [2,3,*]

[1] Postgraduate Department, China Academy of Railway Sciences, Beijing 100081, China; wzeyu1998@163.com
[2] State Key Laboratory for Track Technology of High-Speed Railway, China Academy of Railway Sciences Co., Ltd., Beijing 100081, China; yangdongsheng90@126.com (D.Y.); wzyjoanne@163.com (Z.W.); hayes1213@126.com (M.W.); 18810996585@163.com (Z.C.)
[3] Railway Engineering Research Institute, China Academy of Railway Sciences Co., Ltd., Beijing 100081, China
* Correspondence: zhenhuazhao1980@163.com (Z.Z.); wpwp2012@yeah.net (P.W.)

Abstract

There exist difficulties in applying conventional pre-embedded iron seats and their fastening systems in space-limited areas such as double-slip turnouts. To improve the convenience of fastener installation, a novel K-type pre-embedded iron seat and its fastening system are designed. The anchoring structure of the K-type iron seat is identical to that of the conventional iron seat, while a symmetric structure is adopted at the bolt installation position, reducing the projected area by 43%. Based on the design parameters of the K-type pre-embedded iron seat, finite element models and test specimens are prepared. On this basis, static analysis, pull-out tests, insulation performance tests, and fatigue tests are carried out. Static calculations indicate that the K-type iron seat has the same capacity to bear train loads as the conventional iron seat. The pull-out test results indicate that the pull-out performance of the K-type pre-embedded iron seat meets standard requirements. The insulation performance test results show that, whether under dry or wet conditions, the K-type pre-embedded iron seat and its fastening system maintain good insulation performance, far exceeding the limit of the standard. The fatigue test results demonstrate that the K-type pre-embedded iron seat retains the track gauge well under 3 million loading cycles, complying with standard provisions. The above results demonstrate that the K-type iron seat satisfies the performance requirements specified in standards.

Keywords: double-slip turnout; railway fastening system; pull-out resistance; fatigue performance; electrical insulation; laboratory test

Check for updates

Received: 25 September 2026
Revised: 19 October 2026
Accepted: 21 October 2026
Published: 23 October 2026

Copyright: © 2026 by the authors. Licensee MDPI, Basel, Switzerland. This article is an open access article distributed under the terms and conditions of the Creative Commons Attribution (CC BY) license.

1. Introduction

A double-slip turnout is generally composed of two sets of obtuse crossings, two sets of acute crossings, two sets of switches, and two lead curves, together with the corresponding sleepers, fastening components, switch machines, and circuit equipment. The layout of a double-slip turnout is shown in Figure 1.

Through this complex track structure, a double-slip turnout enables rolling stock to cross and change direction within a limited space, which improves the space utilization efficiency of stations and marshalling yards [1]. Compared with single turnouts, double-slip turnouts contain more movable rail components, which makes coordination among the different components more difficult than with single turnouts [2]. Extensive research has been devoted to the optimization and inspection of double-slip turnouts. Yuan et al. [3]

proposed improvement measures to address the weak geometry retention capability and excessive switch rail wear of double-slip turnouts. Liu [4] designed a No. 9 turnout for the 1520 mm gauge, which solved the interference problem under wide-gauge conditions. Lan [5] proposed suggestions for the layout of double-slip turnouts in metro yards based on existing experiencing. Xie et al. [6,7] analyzed the performance of switch machines with different structural configurations in double-slip turnouts. Kaewunruen [8] developed a type of fiber-reinforced foamed urethane bearer and compared its in-service performance in a double-slip turnout against timber bearers. Qiao et al. [9] established a finite element model of a double-slip turnout on ballasted track, with which the mechanical characteristics of the continuously welded turnout under thermal loads were analyzed. Zhao and Xu [10,11] proposed improvement measures for the point rail locking device of the SC350 double-slip turnout. Kampczyk [12] developed a method for evaluating the geometry of double-slip turnouts using a magnetic measuring square and an electronic total station. Yang and Tian et al. [2,13] analyzed the failures and derailment risks of double-slip turnouts and identified the locations and frequencies of equipment failures using a Bayesian network based on textual data. Wang et al. [14] optimized the guard rail and wing rail interval limits of double-slip turnouts on the basis of field test data. As service time and freight demand increase, the structures of existing double-slip turnouts can hardly meet the requirements of mixed passenger and freight railways in terms of running speed, axle load, and traffic density [15]. In addition, the wide variety of models and structural configurations of existing double-slip turnouts increases operation and maintenance costs. With the aim of unifying these models and improving the service performance of double-slip turnouts, Wang et al. designed a new double-slip turnout that retains the interfaces of existing double-slip turnouts [16].

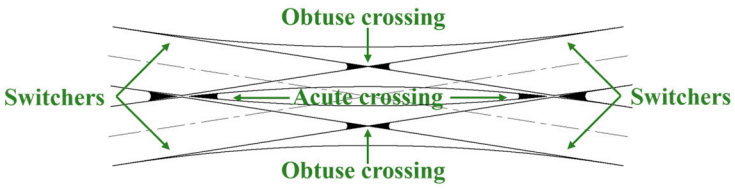


Figure 1. Layout of double-slip turnout.

The complex structure of double-slip turnouts imposes significant restrictions on the installation space available for fasteners and demands the strong ability to maintain geometric alignment. In early railway fastening systems, screw spikes were anchored mainly by anchoring agents such as sulfur mortar, cement mortar, and resin mortar, as shown in Figure 2a. This anchorage approach is associated with severe pollution, long setting times, poor insulation performance [17], and turnout sleeper damage caused by volume expansion [18]. In response to these problems, pre-embedded sleeve fasteners have become the prevailing choice for newly constructed lines [19]. The sleeve is embedded in the concrete, and the rail is fastened to the sleeper using rail spikes, as shown in Figure 2b. This structure prolongs the service life of the sleeve while retaining the insulation capability of the nylon sleeve. Similar technology has found wide application in building construction [20], the installation of large mechanical equipment [21], and other fields.

Pre-embedded sleeves used in railways generally adopt a composite sleeve structure in which a nylon sleeve is pre-installed within a steel sleeve [22]. Sun et al. [23] employed the finite element method to compare the stress states of screw spikes using the sulfur anchorage method and the pre-embedded sleeve method. The results were verified through laboratory tests, and recommendations on the selection of pre-embedded sleeve materials were proposed. Choi and Kim [24] analyzed the causes of failure of the bolts anchored in pre-embedded sleeves in the Korean metro. Jin et al. [25] established a vehicle–

track coupled dynamics model to analyze the loss of pull-out resistance of pre-embedded sleeves in ballast-less track after high-temperature scorching and proposed corresponding maintenance measures.

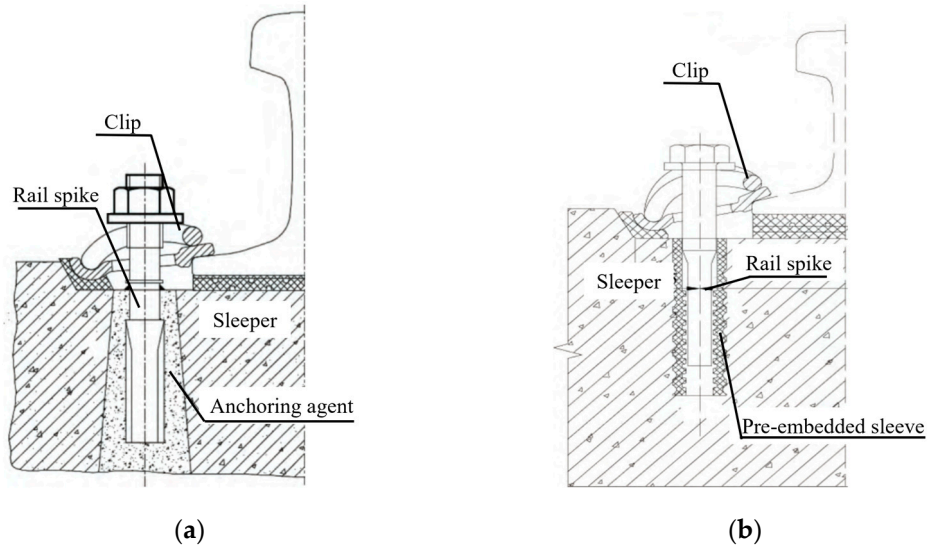


Figure 2. Fastening systems with different anchoring mechanisms: (**a**) anchoring agent; (**b**) pre-embedded sleeve [18].

The track resists lateral forces under train loads through the load transfer path formed by the anchor bolt, the pre-embedded sleeve, and the concrete turnout sleeper. Under the complex wheel–rail forces in the turnout zone, the sleeve is easily damaged, causing failure of its threads and weakening the anchorage capacity of the bolts [26]. In addition, foreign matter such as rain and snow can readily enter the sleeve and form standing water inside during service in cold regions [27]. The accumulated water freezes and expands when the ambient temperature drops below 0 °C, exerting stress on the interface between the sleeve and the concrete turnout sleeper, which finally causes fatigue failure of the sleeve and degrades the pull-out resistance of the fasteners under repeated freeze–thaw. The Type 23 turnout incorporates design experience gained from heavy-haul lines [28,29] and adopts a conventional fastening system with pre-embedded iron seats in place of the pre-embedded sleeve structure [30], as shown in Figure 3.

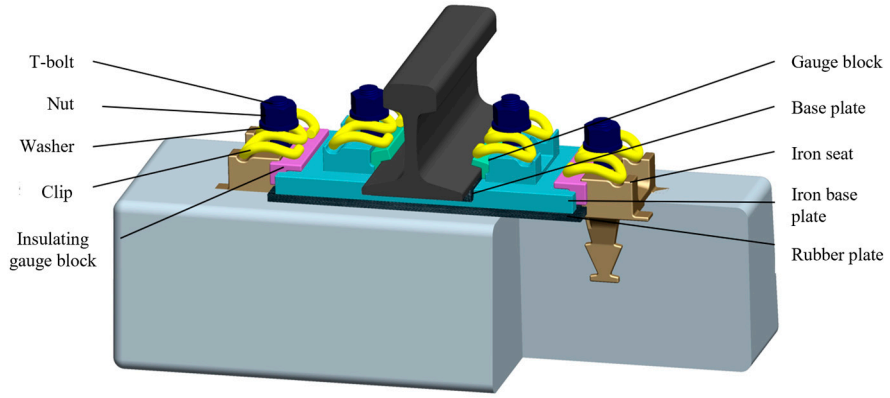


Figure 3. Conventional fastening system with pre-embedded iron seats.

The pre-embedded seat is simpler in structure than the pre-embedded sleeve. Through the anchoring structure, the seat interacts directly with the turnout sleeper, which simplifies the load transfer path and prevents gaps induced by differential shrinkage between

multiple material layers [31]. Similar structures have already been widely applied in large-scale engineering construction [32–34]. Pre-embedded seat fasteners have been widely adopted in fields such as high-speed railways [35], heavy-haul railways [36], and urban rail transit [37].

From the above discussion, it can be seen that current research mostly focuses on the design and defect analysis of pre-embedded iron seats in mainline sections and simple turnout areas, while the design of pre-embedded iron seats for compact layouts and their full-scale tests remain insufficiently investigated. As shown in Figure 4, double-slip turnouts require a large number of turnout components to be accommodated within a limited space, where a single sleeper may support various rail components, including switch rails, stock rails, and nose rails. Consequently, the installation of some rail components in double-slip turnouts is challenging. To facilitate fastener installation and optimize the component layout in double-slip turnouts, a new type of pre-embedded iron seat is proposed in this paper. Its performance is then verified via finite element analysis and laboratory tests to assess whether it satisfies the requirements of standards.

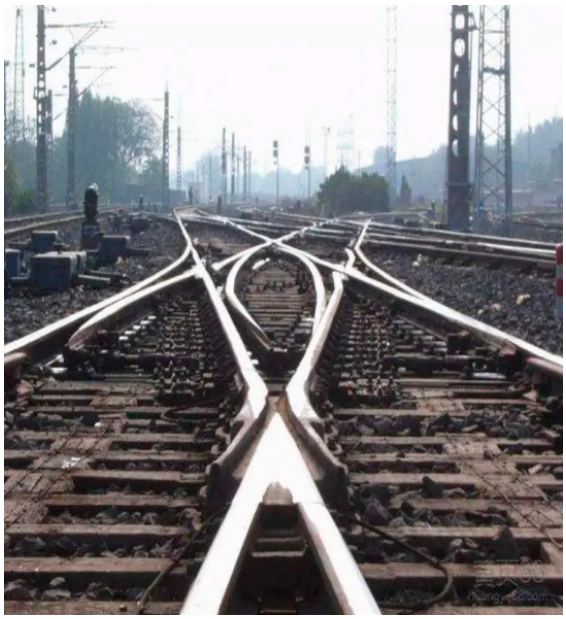


Figure 4. Switching area in a double-slip turnout.

2. Structural Design and Establishment of Finite Element Model for K-Type Pre-Embedded Iron Seat

The large vertical projected area of the conventional pre-embedded iron seat makes it difficult to arrange the different track components in the double-slip turnout. To enable installation in space-limited areas, the K-type iron seat eliminates the structure for placing the clip, and the clip is instead placed on the anti-rotation board, so that one single clip can fasten two adjacent iron baseplates. Above the anchoring structure of the K-type iron seat, only the bolt installation structure is retained. To avoid stress concentration, a rounded fillet design is adopted between the bolt installation structure and the anchoring structure. Insulating gauge blocks are installed between the pre-embedded iron seat and the iron baseplates. The overall structure of the fastening system with the K-type iron seat is shown in Figure 5.

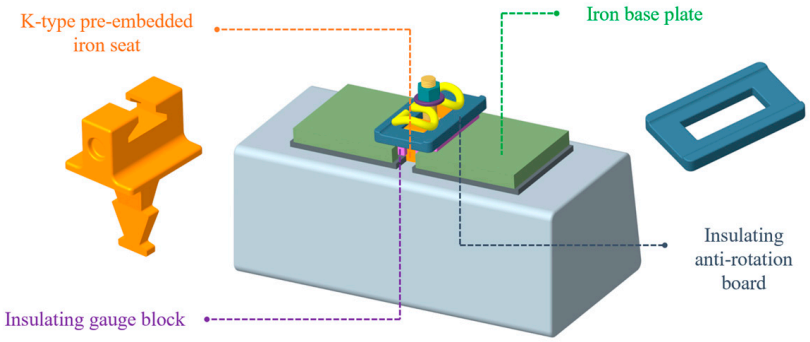


Figure 5. Fastening system with K-type pre-embedded seat.

The K-type pre-embedded iron seat has the same anchoring structure as the conventional fastening system, as shown in Figure 6. The vertical projected area of the bolt fastening system on conventional pre-embedded iron seat is 7752 mm^2. The K-type pre-embedded iron seat employs a symmetric structure at the bolt fastening region, positioned directly above the anchoring structure. The area of its vertical projected region is 4400 mm^2. Compared to the conventional pre-embedded iron seat, this area is reduced by 43%.

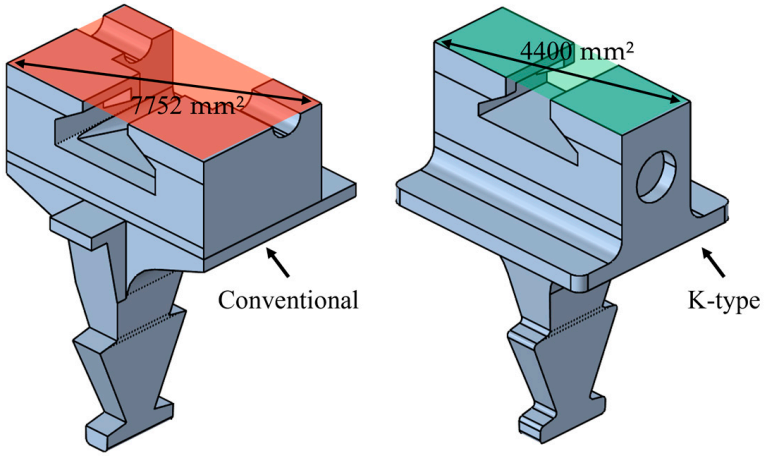
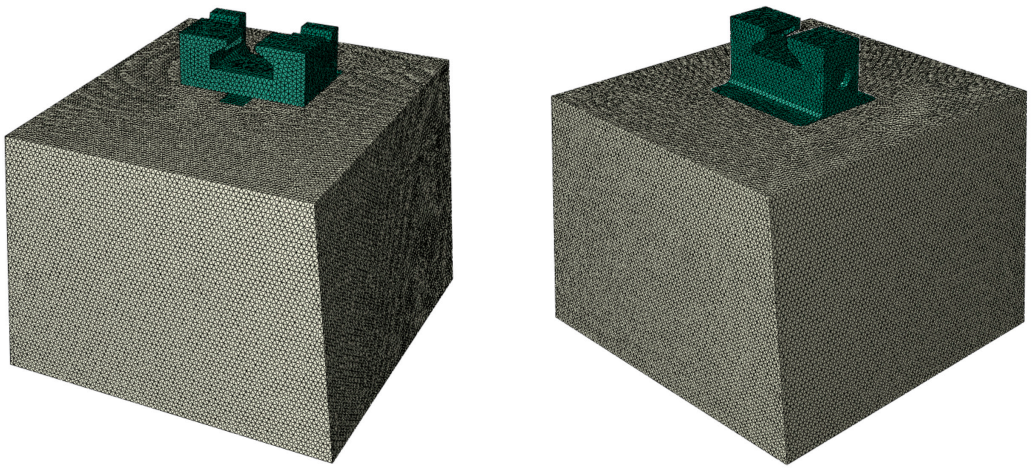


Figure 6. Comparison between 120.3conventional pre-embedded iron seat and a K-type pre-embedded iron seat.

To evaluate the stress level of the K-type pre-embedded iron seat under installation conditions, finite element models of the pre-embedded iron seats of the conventional and K-type fastening system, each including part of the sleeper, are developed, as shown in Figure 7. The finite element models of both types of pre-embedded iron seats are established strictly in accordance with their actual dimensions. Both types of seats are made of ductile iron (QT450-10), with a yield strength of 310 MPa, a tensile strength of 450 MPa, a Young's modulus of 2.1 $\times$ 10^5 MPa, and a Poisson's ratio of 0.3. The sleepers are made of C60 concrete, with a density of 2800 kg/m^3, an elastic modulus of 4.08 $\times$ 10^4 MPa, and a Poisson's ratio of 0.2577. To ensure that the finite element model conforms to the actual geometry of the pre-embedded iron seats, the model is meshed with tetrahedral elements with an element size of 4 mm. To improve computational accuracy, the tet collapse of the tetrahedral elements is maintained above 0.3. The pre-embedded iron seat and the sleeper are connected through a tie constraint.

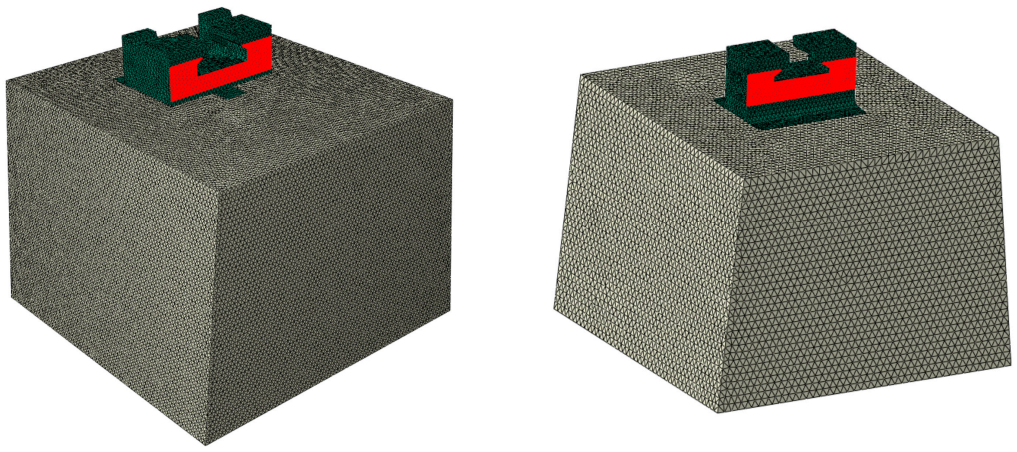


(**a**) (**b**)

Figure 7. Finite element models of pre-embedded iron seats: (**a**) conventional pre-embedded iron seat; (**b**) K-type pre-embedded iron seat.

3. Static Analysis of Pre-Embedded Iron Seat

The pre-embedded iron seat is a key load-transfer component of the fastening system. During train passage, the vertical and lateral loads generated by wheel–rail interaction are transmitted through the rails and fasteners to the pre-embedded iron seat and then to the sleeper. The test results in reference [38] demonstrate that the lateral wheel–rail force of a heavy-haul train passing laterally through the small-number turnout is 99 kN. According to reference [39], the lateral load acting on the fastening system is approximately 65–70% of the lateral wheel–rail force. To analyze the resistance of the K-type iron seat to train loads under the most adverse scenario, a lateral force with a value of 70 kN (70% of 99 kN) is vertically applied at the contact interfaces between the pre-embedded iron seats and the insulating gauge blocks, which is shown as red areas in Figure 8.



(**a**) (**b**)

Figure 8. Lateral load application areas on: (**a**) conventional pre-embedded iron seat; (**b**) K-type pre-embedded iron seat.

The calculation results are shown in Figure 9. The conventional pre-embedded iron seat exhibits a maximum stress at the position where the upper edge of the anchoring structure is in contact with the sleeper. For the K-type pre-embedded iron seat, the maximum stress occurs in the transition region between the bolt fastening location and the upper edge of the anchoring structure. For both types of pre-embedded iron seats, the maximum

stresses in the sleepers all occur at the contact location between the sleeper and the upper edge of the anchoring structure of the pre-embedded iron seat.

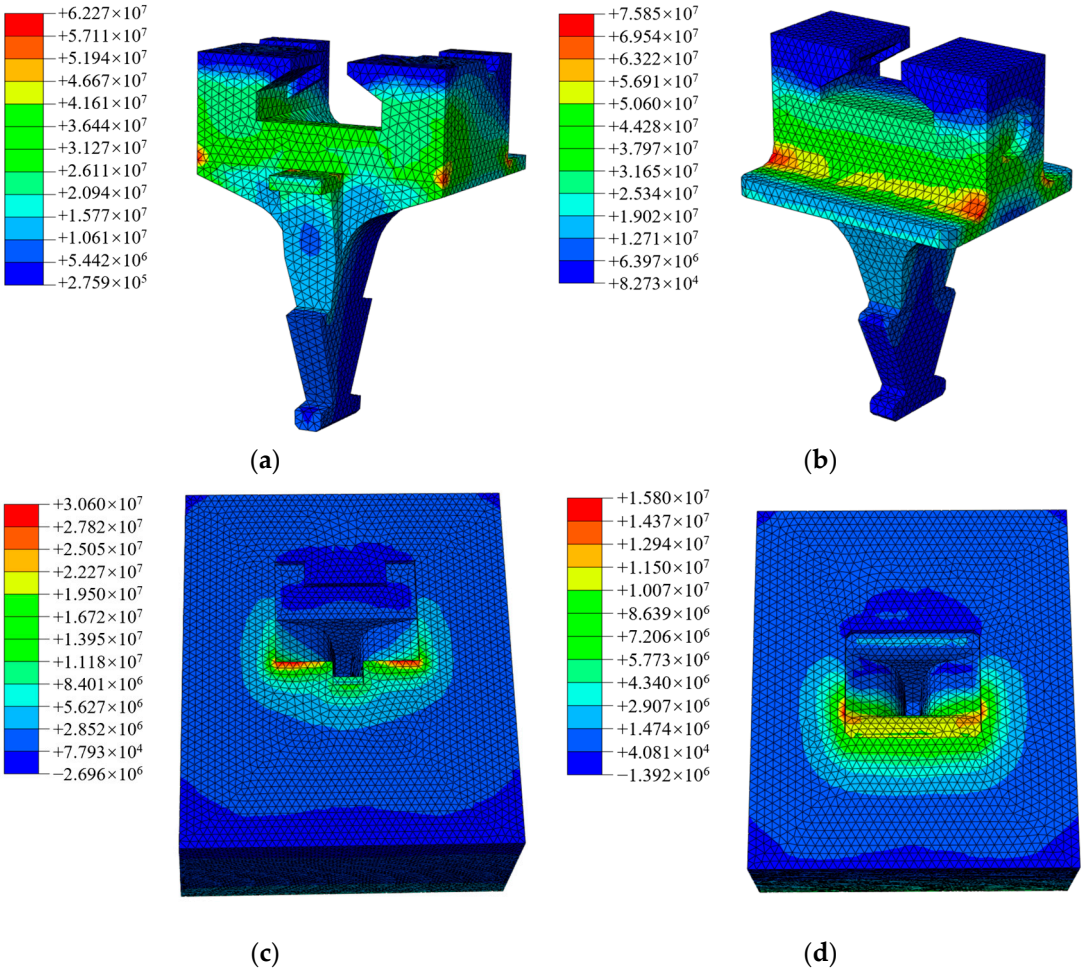


Figure 9. Stress distributions of: (**a**) conventional pre-embedded iron seat; (**b**) K-type pre-embedded iron seat; (**c**) sleeper of conventional fastening system; (**d**) sleeper of K-type fastening system.

The maximum von Mises equivalent stresses of the pre-embedded iron seats and the sleepers are extracted, as shown in Figure 10. The maximum von Mises stresses of the K-type and conventional iron seats are 75.85 MPa and 62.27 MPa, respectively. Although the maximum stress of the K-type iron seat is 13.58 MPa higher than that of the conventional iron seat, it remains below the proof strength of QT450-10 (310 MPa). The maximum principal stresses in the sleepers corresponding to the conventional and K-type iron seats are 30.60 MPa and 15.80 MPa, respectively. Both are compressive stresses and lower than the axial compressive strength of C60 concrete (38.5 MPa). Since the stress differences between the two kinds of iron seat and their sleeper stresses are relatively small and the conventional iron seat has been widely applied on operating lines [29], it can be concluded that the K-type iron seat possesses a load-resisting capacity equivalent to that of the conventional iron seat.

To analyze the pull-out resistance of the pre-embedded iron seats, in accordance with reference [40], a vertical load is applied at the red areas shown in Figure 11a,b. The load is increased from 0 to 60 kN at a rate of 50 kN/min and then held for 180 s. The maximum displacements of sleepers are presented in Figure 11c,d. The maximum sleeper surface displacements corresponding to the conventional iron seat and the K-type iron seat are 1.01 $\times$ 10^{-2} mm and 1.11 $\times$ 10^{-2} mm, respectively, with a difference of

only 0.10×10^{-2} mm. The experimental results in reference [41] indicate that the surface displacement of C60 concrete upon the onset of crack mouth opening is 6.7×10^{-2} mm. Since the calculated sleeper surface displacement amplitudes are smaller than this threshold, it can be concluded that the pull-out resistance of the K-type pre-embedded iron seat is equivalent to that of the conventional pre-embedded iron seat and that cracking of the sleeper surface is unlikely to occur.

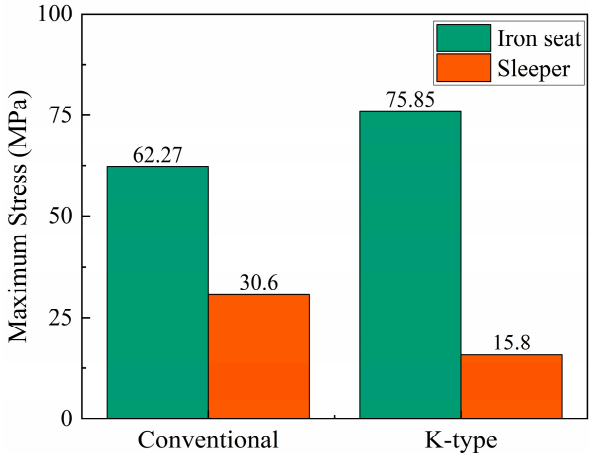


Figure 10. Maximum stresses of pre-embedded iron seats and their sleepers.

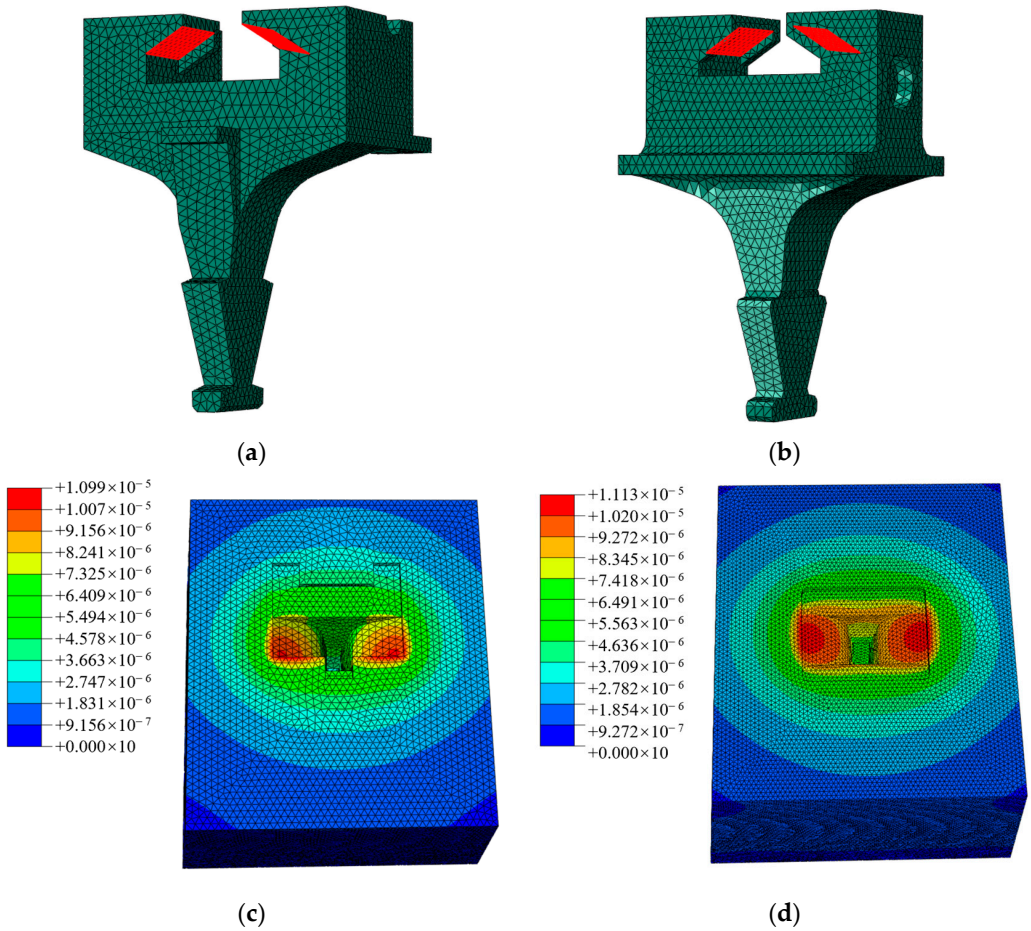


Figure 11. Pull-out resistance analysis of pre-embedded iron seats: (**a**) vertical loading surface on conventional pre-embedded iron seat; (**b**) vertical loading surface on K-type pre-embedded iron seat; (**c**) sleeper surface displacement of the conventional fastening system; (**d**) sleeper surface displacement of the K-type fastening system.

4. Laboratory Test of K-Type Pre-Embedded Iron Seat

To investigate the performance of the K-type pre-embedded iron seat, a K-type iron seat specimen is fabricated, as shown in Figure 12a. In addition, according to the practical layout of the double-slip turnout, a sleeper specimen is fabricated with two kinds of iron seats embedded according to the parameters of sleepers in actual service, as shown in Figure 12b.

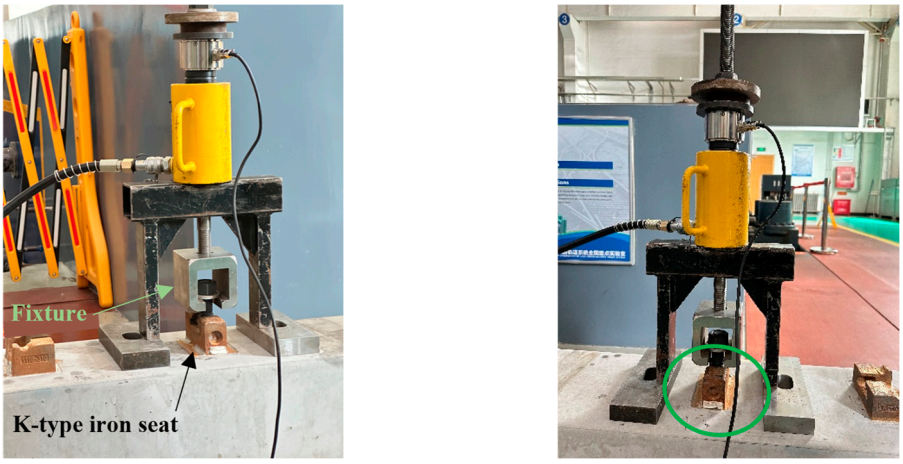


(**a**) (**b**)

Figure 12. Preparation of specimens: (**a**) K-type pre-embedded iron seat; (**b**) sleeper.

4.1. Pull-Out Resistance Test

The pull-out resistance test procedure for the pre-embedded iron seat is specified in references [9,42]. A load vertical to rail seat is applied to the K-type pre-embedded iron seat through a fixture, as shown in Figure 13a. A vertical load is applied at a loading rate of 50 kN/min. After the load reaches 60 kN, it is held for 3 min and then unloads slowly without impact. The condition of the concrete around the K-type iron seat after the test is shown within the area marked by the green circle in Figure 13b. No cracking is observed in the concrete adjacent to the iron seat, which complies with the specifications given in reference [43]. The test proves that the pull-out resistance performance of the K-type pre-embedded iron seat satisfies the requirements of in-service operation.



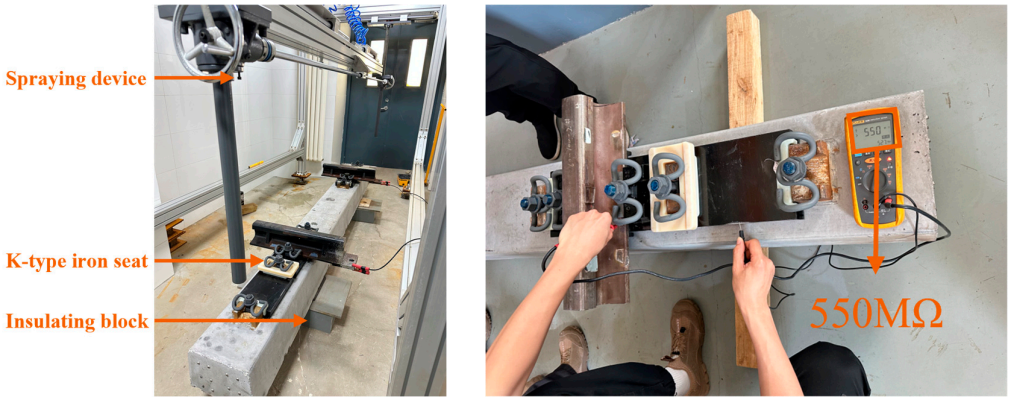
(**a**) (**b**)

Figure 13. Pull-out resistance test: (**a**) test site; (**b**) condition of the sleeper surface after the test.

4.2. Performance of Insulation Test

Following the test in Section 4.1, the rails and their fastening systems are installed above the pre-embedded iron seat of the specimen. To analyze the insulation performance of the K-type pre-embedded iron seat, following the procedure in references [43,44], a spraying device is installed above the rail–sleeper assembly, which is kept insulated from the ground by using wooden blocks and plastic pads. The device has 4 nozzles and delivers

water onto the rail–sleeper assembly at a spray rate of 6–8 L/min for 2 min. During spraying, the electrical conductivity of the water is maintained at 20–80 mS/m and the temperature is maintained at 10–20 °C. Figure 14a shows the test site. The resistance of the assembly in the dry state is 550 MΩ, as shown in Figure 14b.



(**a**) (**b**)

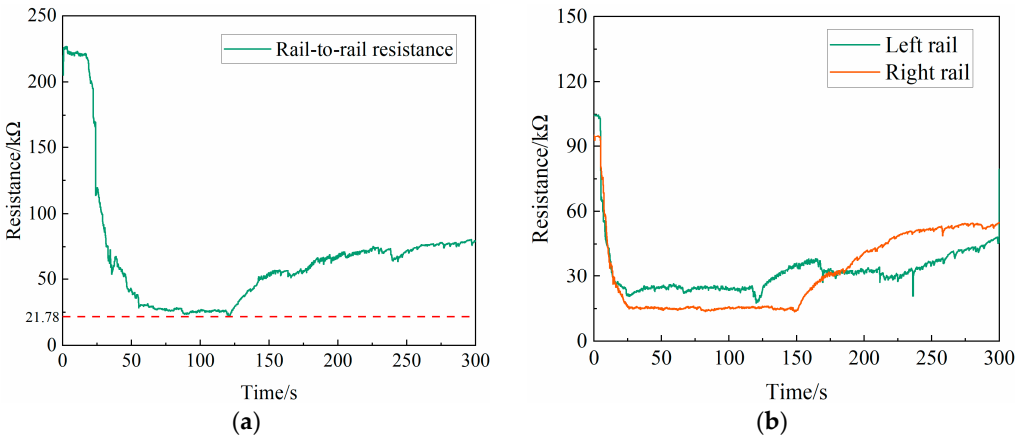
Figure 14. Insulation test: (**a**) spraying device and rail fastener assembly; (**b**) resistance at the initial time.

After spraying, the resistance variation is continuously monitored for 5 min. The minimum resistance is then taken and corrected according to Equation (1) [45]:

$$R_{33} = 0.33 \times \gamma \times R_{\min} \quad (1)$$

where R_{33} is the corrected resistance; γ is the electrical conductivity of the spray water at 25 °C, taken as 50 mS/m in this paper; and $R_{\min}$ is the measured minimum resistance.

The variation in resistance between the two rails is shown in Figure 15a. The resistance first decreases and then increases, eventually stabilizing at about 80 kΩ, with a minimum measured value of 21.78 kΩ. According to Equation (1), the corrected resistance is 32.67 kΩ. The resistance between the rail and the baseplate on one side is measured simultaneously, and the results are shown in Figure 15b. The resistance from both sides of the rails shows a tendency to first decrease and then increase. The minimum resistance of the left rail is 17.66 kΩ and that of the right rail is 13.63 kΩ, which is slightly lower than left rail. The corrected resistance between the rails and their baseplates on the two sides are 26.49 kΩ and 20.45 kΩ, respectively. The test results indicate that the K-type pre-embedded iron seat and its fastening system meet the provision in reference [43], i.e., the resistance between the two rails shall not be less than 3 kΩ.



(**a**) (**b**)

Figure 15. Resistance variations: (**a**) resistance between two rails; (**b**) resistance on a single side.

4.3. Fatigue Test of the Rail–Sleeper Assembly

To analyze the fatigue performance and structural reliability of the K-type pre-embedded iron seat, a fatigue test is performed on the specimen mentioned in Section 4.2 with reference to the requirements in references [43,46]. The test site is shown in Figure 16. Since there exists gauge widening in double-slip turnouts with a maximum value of 5 mm, the gauge of the specimen is adjusted to 1450 mm. The rail is fixed to the sleeper through fastenings, and the K-type pre-embedded iron seat and its fastening system are located on the outer side of the rails. A 38° fatigue test rig is mounted on the tops of both rails. To evaluate the structural reliability of the K-type pre-embedded iron seat under the most adverse scenario in which the K-type iron seat carries the entire lateral load, smaller gauge blocks are installed between the K-type iron seat and the adjacent iron baseplates to create a 2 mm gap, thereby preventing the adjacent iron baseplates from sharing the lateral load. The test parameters are as follows: the vertical and lateral fatigue loads are 60 kN and 75 kN, respectively. The load is applied at a frequency of 3–5 Hz. The height of the rail is 120 mm. The nut of the fastener is further tightened by one quarter of a turn after the front lower jaw of the clip's middle section touches the gauge block.

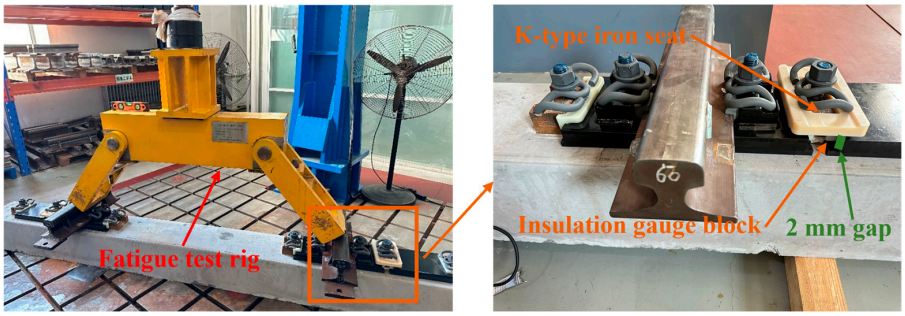


Figure 16. Fatigue test of K-type pre-embedded iron seat.

The total number of fatigue cycles is 3×10^6, conducted in two stages. The first stage consists of 1000 cycles, after which the track gauge is measured. The remaining cycles are applied in the second stage, and the track gauge is measured upon completion of the fatigue test. The variation in the track gauge is illustrated in Figure 17. Compared with the gauge after the first stage, the left-side gauge after 3×10^6 cycles reaches 1450.71 mm with an increase of 0.62 mm. The right-side gauge reaches 1451.88 mm, with an increase of 0.28 mm. The average gauge (the gauge between the two sides of rails) after 3×10^6 cycles is 1451.30 mm, with an increase of 0.45 mm. The increase in the average gauge value complies with the requirement specified in reference [47], i.e., the gauge widening shall not exceed 6 mm.

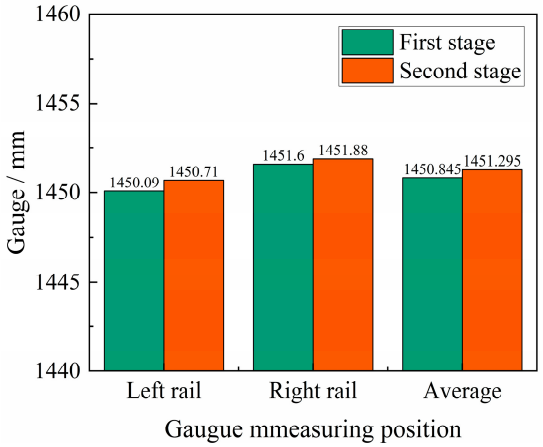


Figure 17. Track gauge variations after the fatigue test.

The aforementioned test results indicate that the pull-out performance, insulation performance, and gauge retention of the K-type pre-embedded iron seat conform to the standard and meet track operation requirements.

5. Discussion

To address the difficulty of installing fasteners in the space-limited areas of double-slip turnouts, this paper proposes a K-type pre-embedded iron seat structure. Its mechanical properties are analyzed using the finite element method. In the new design, the contact position between the insulating gauge block and the pre-embedded iron seat is raised, which increases the moment acting on the seat anchoring structure. Consequently, the stress at the rounded fillet of the K-type iron seat is enlarged under horizontal loads. In this case, the maximum stress of the K-type pre-embedded iron seat is 75.85 MPa, far below the specified proof strength of its material (310 MPa), which ensures the safety of this structure. Laboratory tests show that the pull-out resistance, insulation performance, and gauge retention of the K-type iron seat all satisfy the requirements of existing standards. Compared to the conventional iron seat, the K-type iron seat and its fastening system feature a simplified structure and provide improved installation convenience for double-slip turnouts. Further studies should concentrate on the structural strength and gauge retention ability of the K-type iron seat under in-service train loads, thereby providing a foundation for future design optimization and engineering application.

6. Conclusions

To enable the installation of fastening systems in space-limited areas such as the crossing region of double-slip turnouts, a new K-type pre-embedded iron seat is proposed in this study. Static analysis, pull-out tests, insulation performance tests, and fatigue tests are then conducted on the new pre-embedded iron seat, and the following conclusions are drawn:

(1) The new pre-embedded iron seat adopts the same anchoring structure as the conventional pre-embedded iron seat, but with a symmetric structure at the bolt anchoring positions. The vertical projected area of iron seat is reduced by 43% and the load transfer path is optimized, which improves the convenience of installing fastenings in space-limited areas.

(2) The static analysis results reveal that under lateral loads, the stress level of the K-type pre-embedded iron seat is close to that of the conventional pre-embedded iron seat, with a difference of 13.58 MPa. The pull-out resistance of the K-type pre-embedded iron seat is consistent with that of a conventional pre-embedded iron seat. Under vertical loads, the difference in the maximum sleeper surface displacement is only 0.10×10^{-2} mm.

(3) The insulation performance test results show that in the dry state, the K-type pre-embedded iron seat and its fastening system exhibit good insulation performance, with an initial resistance of 550 MΩ. In the wet state, the resistance of the fastening system decreases: the equivalent resistance between the two rails is 32.67 kΩ, and the equivalent resistances between each rail and its baseplate are 26.49 kΩ and 20.45 kΩ, respectively, all of which remain higher than the requirement of 3 kΩ in the specification.

(4) The fatigue test results demonstrate that after 3 million loading cycles, the K-type pre-embedded iron seat shows good gauge retention ability. The increase in average gauge is 0.45 mm, which is less than the standard limit of 6 mm.

(5) The results of the numerical analysis and laboratory tests indicate that the K-type pre-embedded iron seat meets the performance requirements specified in standards.

Author Contributions: Conceptualization, Z.W. (Zeyu Wu) and Z.Z.; methodology, Z.W. (Zhongyuan Wang) and D.Y.; software, Z.W. (Zeyu Wu); validation, Z.W. (Zhongyuan Wang) and M.W.; formal analysis, Z.W. (Zeyu Wu); investigation M.W.; resources, D.Y.; writing—original draft preparation, Z.W. (Zeyu Wu); writing—review and editing, Z.C.; supervision, P.W. and Z.Z.; project administration, P.W.; funding acquisition, P.W. All authors have read and agreed to the published version of the manuscript.

Funding: The research described in this paper was financially supported by the foundation program of the China Railway (K2026G019), the National Natural Science Foundation of China (52608778), and the foundation program of the China Academy of Railway Sciences (2025YJ185).

Institutional Review Board Statement: Not applicable.

Informed Consent Statement: Not applicable.

Data Availability Statement: The original contributions presented in this study are included in the article. Further inquiries can be directed to the corresponding author.

Conflicts of Interest: Authors Dongsheng Yang, Zhongyuan Wang, Meng Wang, Zelin Chen, Zhenhua Zhao, and Pu Wang were employed by the Railway Engineering Research Institute, China Academy of Railway Sciences Co., Ltd. The remaining authors declare that the research was conducted in the absence of any commercial or financial relationships that could be construed as a potential conflict of interest.

References

1. Wang, P. *Design of High-Speed Railway Turnouts: Theory and Applications*; Academic Press: Cambridge, MA, USA, 2015; ISBN 978-0-323-39617-2.
2. Tian, S.; Qi, J.; Wang, B.; Wang, K. Fault diagnosis of double slip switches based on Bayesian network. *J. Beijing. Jiaotong. Univ.* **2020**, *44*, 118–125.
3. Yuan, B.; Liu, Q. Improved design on Number 12 Double Slip Points in 60 kg/m Track. *Railw. Stand. Des.* **2006**, 10–11. [CrossRef]
4. Liu, Q. Design of No. 9 double slip turnout with 50 kg/m rail for 1520 mm gauge. *Railw. Stand. Des.* **2008**, 10–13.
5. Lan, S. Solutions to Relative Problems in Design of Station Yard of Metro Vehicle Depot. *J. Railw. Eng. Soc.* **2010**, *27*, 119–122.
6. Xie, Z. Research on the Application of Double-rod Switch Machines in Double Slip Turnouts. *Railw. Signal. Commun. Eng.* **2010**, *7*, 62–64.
7. Zhou, F. Application of ZD9-S Double Rod Point Machine in Double Slip Switches. *Railw. Signal. Commun. Eng.* **2018**, *15*, 84–86.
8. Kaewunruen, S. Monitoring In-Service Performance of Fibre-Reinforced Foamed Urethane Sleepers/Bearers in Railway Urban Turnout Systems. *Struct. Monit. Maint.* **2014**, *1*, 131. [CrossRef]
9. Qiao, S.; Gao, L.; Cheng, Y. Mechanical characteristics and seamless research of double slip switches. *J. Beijing. Jiaotong. Univ.* **2012**, *36*, 61–65.
10. Zhao, Y. Optimization and Improvement of Point Rail Indication for SC350 Double Slip Turnout. *Railw. Signal. Commun.* **2019**, *55*, 17–19.
11. Xu, J. Optimization and Improvement of Point Rail External Locking for SC350 Double Slip Turnout. *Railw. Signal. Commun.* **2019**, *55*, 11–14.
12. Kampczyk, A. Measurement of the Geometric Center of a Turnout for the Safety of Railway Infrastructure Using MMS and Total Station. *Sensors* **2020**, *20*, 4467. [CrossRef] [PubMed]
13. Yang, L.; Li, K.; Song, G.; Khan, F. Dynamic Railway Derailment Risk Analysis with Text-Data-Based Bayesian Network. *Appl. Sci.* **2021**, *11*, 994. [CrossRef]
14. Wang, P.; Wang, S.; Zhao, Z. Mechanism of Derailment at the Guardrail Position of Turnout and a Reasonable Guardrail Interval Limit. *Appl. Sci.* **2022**, *12*, 8496. [CrossRef]
15. Wang, S.; Ge, J.; Si, D.; Wang, M. Study on Guard Check Gauge of Fixed Frog and Design on Widening Nose Rai. *China Railw. Sci.* **2014**, *35*, 7–12.
16. Wang, S.; Wang, P.; Zhao, Z.; Yang, D.; Wang, M.; Wang, Z.; Ge, J.; Si, D.; You, R.; Li, J. Overview of Key Technology Research on Design of "Type 23" Mixed Passenger and Freight Railway Turnouts. *J. China Railw. Soc.* **2026**, *48*, 56–72.

17. Li, S.; Li, B.; Fang, H.; Cheng, G.; Han, B.; Shu, S.; Xia, S. Application Status of Screw Spike Anchoring Materials for Concrete Sleeper. *Railw. Eng.* **2021**, *61*, 133–137.
18. Duan, Y.; Chen, P.; Sun, D.; Xu, S.; Duan, H. Development of a New Embedded-Sleeve Rail Fastening System for Ballasted Track. *Urban Rapid Rail Transit* **2025**, *38*, 124–128.
19. He, Y.; Xiao, Z.; Zhang, Y. Application Status and Structural Optimization Measures of Intersecting Crossover Turnout. *Railw. Eng.* **2024**, *64*, 32–36.
20. Ke, M. Research on the Key Technology of Embedded Nylon Casing in Tunnel by Mining Method. *J. Phys. Conf. Ser.* **2020**, *1676*, 012007. [CrossRef]
21. Wang, Z.; Wu, Y.; Liu, H.; Fan, Z.; Zhao, J. Construction Technology for Controlling Installation Accuracy of Pre-embedded Casing in Steam Turbine Foundation. *Value Eng.* **2022**, *41*, 126–128.
22. Liu, X.; Sun, H.; Zhang, L.; Ma, J. Research and Application of New Fastening Systems for Mixed Traffic Railways. *Railw. Stand. Des.* **2025**. [CrossRef]
23. Sun, L.; Fang, H.; Ran, L.; Liu, W.; Kong, Q. Stress Analysis of Screw Spike in Type II Fastening System. *Railw. Eng.* **2019**, *59*, 129–133.
24. Choi, J.; Kim, B. Failure Analysis of Anchor Bolt of Rail Fastening System for Direct Fixation Track. *Eng. Fail. Anal.* **2020**, *112*, 104513. [CrossRef]
25. Jin, H.; Yang, Y.; Zhao, X.; Pan, Y.; Chu, J.; Li, S.; Xu, S.; Feng, Y. Changes in Material Properties and Damage Mechanism of Plate Ballastless Track Under Fire and High Temperature. *Buildings* **2025**, *15*, 1987. [CrossRef]
26. Wang, Y. Analysis of Advantages and Disadvantages Between Embedded Sleeves and Embedded Iron Seats in Railway Switch Sleepers. *Railw. Constr. Technol.* **2026**. [CrossRef]
27. Teng, D. Research on Maintenance Technology for CRTS I Slab Ballastless Track in Severe Cold Regions. *Railw. Eng.* **2013**, 127–130.
28. Wang, S.; Ge, J.; Wang, M.; Chao, J. Design of No.12 Turnout in Heavy Haul Railway. *Railw. Eng.* **2013**, 98–102.
29. Wang, M.; Yang, D.; Si, D. Research and Application of Key Technologies of Heavy Haul Railway Turnouts. *China Railw.* **2020**, 105–110.
30. Zhao, Q.; Wang, Z.; Wu, Z.; Ge, J.; Wang, P. Design for 60 kg/m Rail No.9 Scissors Crossover of Mixed Passenger and Freight Railway and Its Verification. *Railw. Eng.* **2025**, *65*, 39–44.
31. Gou, X.; Wang, H.; Ma, L.; Chen, Y.; Li, F. Work Principle and Selection Analysis of Waterproof Casings. *Water Wastewater Eng.* **2023**, *59*.
32. Liang, Y.; Zhang, Y.; Tan, J. Experimental Investigation of the Pull-Out Behavior of Semi-Embedded Anchor Bolts in Concrete Transition Sections. *Buildings* **2026**, *16*, 3105. [CrossRef]
33. Wu, T.; Huang, F.; Zhang, D.; An, Y. Anchorage Failure Mechanism and Uplift Bearing Capacity of L- & J-Anchor Bolts in Plain Concrete. *Eng. Fail. Anal.* **2024**, *159*, 107991. [CrossRef]
34. Karmokar, T.; Mohyeddin, A.; Lee, J.; Paraskeva, T. Concrete Cone Failure of Single Cast-in Anchors under Tensile Loading—A Literature Review. *Eng. Struct.* **2021**, *243*, 112615. [CrossRef]
35. Liu, C. Study on Optimization of Large Height Adjustment Capacity of Existing Embedded Iron Seat Fastener. *Railw. Eng.* **2021**, *61*, 126–129.
36. He, X.; Xu, Y.; Ran, L. Design and Research on Embedded Iron Base for Heavy Haul Railway Turnout. *Shanxi Archit.* **2018**, *44*, 134–135.
37. Zhang, Z.; Huang, Q. Design and Research of Vibration Absorbing Fasteners for No. 9 Turnout of Urban Rail Transit. *Railw. Stand. Des.* **2020**, *64*, 13–17.
38. Wang, S. Research on the Key Technologies of Prolonging the Service Life of Heavy-Haul Turnouts. Doctoral Dissertation, China Academy of Railway Science, Beijing, China, 2015.
39. Chen, X.; Lou, P. *Railway Engineering*, 2nd ed.; China Architecture and Building Press: Beijing, China, 2015.
40. Zeng, Z. Technical Parameters and Test Methods of Sleepers Made of Fiber Reinforced Polymer. *Railw. Eng.* **2021**, *61*, 107–112.
41. Chen, H.H.; Su, R.K.L. Tension Softening Curves of Plain Concrete. *Constr. Build. Mater.* **2013**, *44*, 440–451. [CrossRef]
42. *EN 13146-10*; Railway Applications-Track-Test Methods for Fastening Systems-Part 10: Proof Load Test for Pull-out Resistance. European Committee for Standardization: Brussels, Belgium, 2017.
43. Shao, T.; Li, C.; Liu, H.; Niu, J.; Zhang, C.; Yu, D. Design of small radius curve fastener optimization scheme for mixed passenger and freight railway. *Railw. Eng.* **2026**, *66*, 79–84.
44. *EN 13146-5*; Railway Applications-Track-Test Methods for Fastening Systems-Part 5: Determination of Electrical Resistance. European Committee for Standardization: Brussels, Belgium, 2012.
45. Shu, R.; Chen, Z.; Yang, J.; Chen, Z. Structural Optimization and Experimental Study of Reinforced RPC Sleeper for Rack Railways. *Railw. Stand. Des.* **2026**, *70*, 48–53.

46. *EN 13146-4*; Railway Applications-Track-Test Methods for Fastening Systems-Part 4: Effect of Repeated Loading. European Committee for Standardization: Brussels, Belgium, 2020.
47. Shao, T.; Li, C.; Liu, H.; Niu, J.; Zhang, C.; Yu, D. Research on fastener system design for small-radius curves in mixed passenger and freight railways. *Railw. Eng.* **2026**. [CrossRef]

Disclaimer/Publisher's Note: The statements, opinions and data contained in all publications are solely those of the individual author(s) and contributor(s) and not of MDPI and/or the editor(s). MDPI and/or the editor(s) disclaim responsibility for any injury to people or property resulting from any ideas, methods, instructions or products referred to in the content.